Desalination and Water Treatment
www.deswater.com

doi: 10.5004/dwt.2017.20715

74 (2017) 237–247
May

Fabrication of functional macroscopic polymer microtubes from *N*,*N*′-methylene bisacrylamide crystals and their adsorption for Cr(VI)

Yaqing Zhang[a], Botian Li[b], Liming Tang[a,*]

[a]*Key Laboratory of Advanced Materials of Ministry of Education of China, Department of Chemical Engineering, Tsinghua University, Beijing 100084, China, Tel. +(86) 13520654252; email: tanglm@tsinghua.edu.cn (L. Tang), Tel. +(86) 15201520774; email: zhangyaq14@mails.tsinghua.edu.cn (Y. Zhang)*
[b]*Department of Materials Science and Engineering, China University of Petroleum, Beijing 102249, China, Tel. +(86) 13426108042; email: libotian2012@sina.cn*

Received 28 November 2016; Accepted 18 March 2017

ABSTRACT

In this article, functional macroscopic polymer microtubes were fabricated via two preparation steps. First, the reversible addition–fragmentation chain transfer polymerization of *N*,*N*′-methylene bisacrylamide (MBA) crystals directly, and then the modification of the resulting polymer tubes. Because the polymerization was confined at the outer layer of the crystals, polymer microtubes were successfully prepared after extracting MBA molecules from crude product by ethanol. Owing to the large size of the crystals, low temperature and high amount of initiator should be adopted to achieve adequate morphology for the tubes. The polymer microtubes were further reacted with tetraethylenepentamine (TEPA) in ethanol based on aza-Michael addition between acrylamide groups and amino groups. The existence of TEPA segments in the modified polymers was confirmed by Fourier-transform infrared, elemental analysis, thermogravimetric analysis and swelling ratio measurements. The modified polymer microtubes displayed high hydrophilicity and could be used as absorbent for Cr(VI) in water. The adsorption capacity increased as decreasing pH value and reached the maximum at pH 2.5. The maximum adsorption capacity was estimated to be 95.2 mg/g by Langmuir adsorption model which fitted the data quit well. The modified polymer microtubes displayed good recycling performance as well.

Keywords: RAFT polymerization; Methylene bisacrylamide crystal; Macroscopic polymer microtube; Supramolecular chemistry; Adsorption of Cr(VI)

1. Introduction

As a kind of hazardous ions, Cr(VI) is fatal to many living organisms [1]. It widely exists in wastewater from chromium metal production, electroplating, leather tanning, dying, etc [2,3]. The concentration of Cr(VI) in wastewater is usually 50–100 mg/L [4], while the maximum permissible concentration was set at 200 μg/L [5]. Therefore, the wastewater must be treated before being discharged into the environment. During the past decade, various technologies have been adopted to extract Cr(VI) from wastewater, including chemical precipitation [4], solvent extraction [6], membrane filtration [7], adsorption [8] and so on. Among them, adsorption is highly attractive due to its advantages of simplicity and effectiveness. In these years, many different adsorbents for Cr(VI) have been reported. However, most of them are in the shapes of particles and spheres [9,10]. It is desired to develop new adsorbents with simple preparation process and improved adsorption capacity.

As a well-known controlled/living radical polymerization method, reversible addition–fragmentation chain transfer (RAFT) polymerization has been investigated extensively during the past decade because of the capability to prepare polymers with uniform molecular weight and controlled molecular architectures [11–13]. Based on macromolecular assembly, the resulting polymer chains have been explored to build a variety of nanostructured functional polymeric

* Corresponding author.

materials, such as micelles, vesicles, nanoparticles and so forth [13–15]. However, the structures of the nanosized objects are often difficult to modulate because of the dynamic assembling process [14]. If the monomers assembled into highly ordered entities in advance, the polymerization would result in well-shaped polymer structures directly. For example, photopolymerization of the organogels of polymerizable urea derivative enabled the formation of fibril structures similar to the assembling fibers [16]. However, it is still a challenge to preserve the assembling structures during the polymerization process, especially at macroscopic scale.

Polymer microtubes and nanotubes have demonstrated potential applications in drug delivery [17], separations [18], catalyst carrier [19], photoluminescence properties [20] and so forth. They could be fabricated mainly via template-free methods and template methods. The later methods included hard template method [21], soft template method [22] and electrospinning method [23]. However, the template must be removed after forming the tubes. Recently, we described a novel process to fabricate polymer microtubes via RAFT polymerization of *N*,*N*′-methylene bisacrylamide (MBA) xerogel fibers as both templates and monomer source [24–27]. Using this strategy, polymer microtubes tethered by polymer nanowire networks [28] and fluoropolymer microtubes were also prepared [29]. The mechanism investigation revealed that RAFT polymerization was critical for the formation of polymer tubes [27,28], because it increased intermolecular crosslinking and the interlacing of the polymer chains, thus to form crosslinked polymer layer covering the templates [13,30], while the conventional free-radical polymerization preferred to form polymer particles under identical conditions [31,32]. However, supramolecular gels could be formed only with specific monomers in suitable solvents, for example, MBA in chloroform [33]. The fabrication of xerogel fibers from the gels is often complicated and time consuming. These shortcomings limited the application of this process considerably. On the other hand, large sized MBA acicular crystals could be fabricated in large quantity at a time simply via recrystallization process. If MBA crystals could be applied directly in the preparation of polymer tubes, this process would become simpler.

Recently, we tried to fabricate functional macroscopic polymer microtubes via two preparation steps, including the RAFT polymerization of MBA crystals and the modification of the resulting tubes. The influence of reaction conditions on the morphologies and weight of products were investigated. The resulting polymer microtubes were further modified with tetraethylenepentamine (TEPA) via aza-Michael addition between acrylamide groups and amino groups [34]. Due to the existence of TEPA segments, the modified polymer microtubes displayed high adsorption capacity for Cr(VI), with the maximum adsorption capacity at 95.2 mg/g, which is higher than those of most reported absorbents. The absorbed Cr(VI) could be desorbed in sodium hydroxide solution as well, which provided good recycling performance for the modified sample. To the best of our knowledge, this should be the first time to fabricate macroscopic polymer microtubes from acicular crystals. Considering the simple preparation process, high adsorption capacity and good recycling performance, this preparation process might be applied to fabricate many other functional macroscopic objects.

2. Experimental setup

2.1. Materials

MBA (LANYI, Beijing, China, 99.0%), TEPA (Sinopharm Chemical Reagent Co., Ltd., Shanghai, China, 90.0%) and $K_2Cr_2O_7$ (Beijing Chemical Works, Beijing, China, 99.8%) were used as received. Dibenzyl trithiocarbonate (DBTTC, RAFT reagent) was synthesized according to the literature [35]. Azodiisobutyronitrile (AIBN; Shanghai No.4 Reagent & H.V. Chemical Co., Ltd., Shanghai, China, 98%) were recrystallized from ethanol and dried under vacuum before use. 1,5-Diphenylcarbazide (Alfa Aesar, Shanghai, China, 97%), hydrochloric acid (Yongfei Chemical Works, Tianjing, China, 37%) and sodium hydroxide (Beijing Chemical Works), pyridine (Beijing Chemical Works, 99.5%), ammonium hydroxide (Beijing Chemical Works, 26%), toluene (Beijing Chemical Works, 99.5%) and ethanol (Beijing Chemical Works, 99.7%) were used as received.

2.2. Measurements

Scanning electron microscopy (SEM) images were obtained by a JSM 7401 field-emission scanning electron microscope with an operating voltage of 3 kV. The samples were prepared on electroconductive paste sprayed by gold powder. Infrared (IR) spectrum was recorded, and Fourier-transform infrared (FTIR) spectrum was measured on a Nicolet 560 FTIR spectrometer. Elemental analysis was performed by using a Vario EL III element analyzer (Elementar, Shanghai, China). Thermogravimetric analysis (TGA) was measured by a DTG-60 thermogravimetric analyzer (Shimadzu, Suzhou, China). The test was conducted from room temperature to 700°C at the heating rate of 5°C/min under nitrogen protection (25 mL/min). Microphotographs were obtained by an Eclips E200 optical microscope (Nikon, Shanghai, China) at the magnification times of 400. Samples were measured in a Y-type cuvette with optical path length of 1 cm. The solubility of MBA in toluene was measured by magnifying the experimental condition with 10 times. MBA (0.9 g) was mixed with toluene (60 g) at different temperatures under stirring. After hot filtration and vacuum drying, the solubility was calculated according to the weight difference. Water contact angles were measured by a JC2000C1 contact angle tester. The swelling ratio was calculated by the equation: swelling ratio = $(w_1 - w_2)/w_1$, where w_1 represents the weight of dry sample; and w_2 represents the weight of wet sample after being immerged into solvent for 24 h at 25°C. Concentration of Cr(VI) was measured by the standard colorimetric method [36] with the wavelength at 540 nm by a UV-3200 spectrophotometer (Mapada Instruments, Shanghai, China). Adsorption or desorption capacity was calculated by Eq. (1):

$$q_e = \frac{(c_0 - c_e) \times V}{m} \tag{1}$$

where q_e is the equilibrium adsorption/desorption capacity (mg/g); c_0 and c_e are initial and equilibrium concentration of Cr(VI) (mg/L), respectively; V is the volume of Cr(VI) solution (mL); m is the weight of polymer microtubes (mg).

Langmuir adsorption model and Freundlich adsorption model were applied to analyze the adsorption isotherms as Eqs. (2) and (3):

$$\frac{c_e}{q_e} = \frac{1}{K_L q_m} + \frac{c_e}{q_m} \quad (2)$$

$$\log q_e = \log K_F + (1/n)\log c_e \quad (3)$$

where Langmuir constants q_m and K_L are referred to maximum adsorption capacity and apparent heat change respectively; K_F and n are the constants of Freundlich isotherm.

2.3. Fabrication of PMBA microtubes

The MBA monomer purchased from factory was in the form of either powder or acicular crystals. To obtain uniform acicular crystals, 3.0 g MBA was dissolved in acetone (150 mL) at 55°C and recrystallized at 5°C for 24 h. The poly(methylene bisacrylamide) (PMBA) microtubes were prepared by RAFT polymerization. A typical procedure for preparing sample 1 (Table 1) is as follows. AIBN (0.0090 g) and DBTTC (0.0130 g) were added into a vial and dissolved in toluene (6.0 g) by ultrasonic dispersion. The solution with initiator and RAFT reagent was mixed with MBA acicular crystals (0.090 g) in another vial. After degassing by argon for 30 min and sealing by rubber plug and Teflon tape, the vial was heated in an oil bath controlled at 65°C. After 48 h of polymerization, the vial was cooled at room temperature and exposed to air in order to terminate the reaction. The solid yellowish product was taken out from the vial, washed by ethanol for three times and dried in a vacuum oven for 24 h. Experiments were conducted under different conditions as shown in Table 1.

2.4. Synthesis of modified polymer microtubes

The modification of sample 1 (Table 1) is listed below: the polymer microtubes (0.0342 g) and TEPA (0.5 g) were mixed with ethanol (7.0 g) in a vial. The reaction was conducted under magnetic stirring at room temperature for 24 h. The stirring rate was relatively low in order not to break the microtubes. The product was separated and washed by ethanol for four times. After dried in a vacuum oven for 24 h, the modified polymer microtubes (0.0318 g) was obtained as white solid.

Table 1
Conditions for RAFT polymerization of MBA crystals and weight of products[a]

Sample	AIBN (g)	DBTTC (g)	T (°C)	Weight of product (g)
1	0.0090	0.0130	65	0.0172
2	0.0090	0.0130	60	0.0045
3	0.0090	0.0130	70	0.0179
4	0.0090	0.0130	75	0.0316
5	0.0090	0.0130	80	0.0317
6	0.0027	0.0130	80	0.0156
7	0.0090	0.0000	65	0.0811
8	0.0090	0.0065	65	0.0281
9	0.0090	0.0200	65	0.0167
10	0.0040	0.0130	65	0.0103
11	0.0060	0.0130	65	0.0134
12	0.0120	0.0130	65	0.0212
13	0.0150	0.0130	65	0.0273
14	0.0180	0.0130	65	0.0327

[a]Conditions: 0.0900 g MBA, reacted for 48 h.

2.5. Adsorption and desorption of Cr(VI)

The $K_2Cr_2O_7$ aqueous solution (50 mg/L) was used to measure the adsorption capacity of modified polymer microtubes. A suitable amount of polymer microtubes (0.0050 g) was added into solution of Cr(VI) (5 mL) in a vial. The solution pH value was adjusted to 2.0–11.5 by diluted hydrochloric acid or sodium hydroxide solution. The adsorption was conducted at 35°C for 24 h. While 0.1 mol/L sodium hydroxide solution was used for desorption of Cr(VI). The solid sample and solution were separated by centrifuge or filter. The concentration of Cr(VI) ions in solution was measured by the standard colorimetric method [36]. After acidification of samples with 1 mL diluted hydrochloric acid and mixing with 1,5-diphenylcarbazid, a purple colour solution was obtained. The UV absorbance at 540 nm was measured by a UV–Vis spectrophotometer to determine the concentration of Cr(VI).

3. Results and discussion

3.1. Fabrication of PMBA microtubes

In our previous article, small sized PMBA polymer microtubes were fabricated via RAFT polymerization of MBA xerogel fibers as both templates and monomer source [24–26]. To obtained macroscopic polymer microtubes, we carried out the RAFT polymerization of MBA crystals directly, which could be obtained in large quantity via recrystallization.

The morphologies of MBA crystals and the typical PMBA microtubes (Table 1, sample 1) were imaged by SEM. Fig. 1(a) shows that the average diameter of MBA crystals is about 11.0 μm. Because the crystals are fragile and easy to be broken, the polymerization should be carried out without stirring. Fig. 1(b) shows the morphology of the crude product before washing by ethanol, which reveals fiber-like structure with solid core. After being washed by ethanol, the fibers turned into microtubes with hollow structure and smooth interior surface. Fig. 1(c) indicates that the resulting PMBA microtubes have relatively uniform diameter of about 11.0 μm, corresponding well to the diameter of MBA crystals. Moreover, the average thickness of the tube wall is about 0.4 μm, which indicates that the polymerization was confined at the outer part of the crystals to give a crosslinked polymer layer covering the core. The obtained PMBA

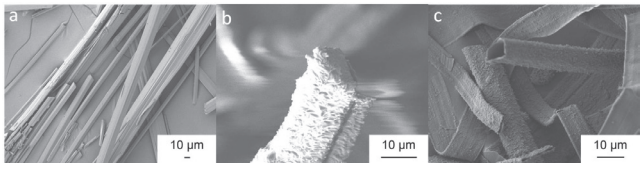

Fig. 1. SEM images of: (a) MBA crystals; (b) crude product of sample 1 and (c) PMBA microtubes of sample 1.

microtubes could be seen by naked eyes (Fig. S1 in supporting information) and operated individually. Because most of the MBA molecules kept unreacted, the weight of product is only 0.0172 g (sample 1) for 0.0900 g MBA crystals. The unreacted MBA monomer could be extracted by ethanol and purified for further reaction. Since the actual conversion of MBA was difficult to determine, the weight of product was used to discuss the reaction extent in the following text.

In our previous article, RAFT polymerization of MBA xerogel fibers with diameter of 1.1 μm was optimally carried out at 82°C, 0.0085 g RAFT reagent and 0.0020 g AIBN [26]. Because the diameter of MBA crystals is much larger than that of MBA xerogel fibers, the reaction conditions should be adjusted to achieve adequate tube morphologies.

The reaction temperature played a major role in polymerization process because it determined the decomposition rate of AIBN, the solubility of MBA in toluene and thus the polymerization rate. Table 2 indicates that the solubility of MBA in toluene became larger as increasing the temperature. The influence of reaction temperature on the morphologies of the tubes is shown in Fig. 2. At the lowest temperature of 60°C, the tubes collapsed into belts because of the thin wall, as shown in Fig. 2(a). From Fig. 2(b), the tubes obtained at 65°C demonstrate self-support ability because of their thick wall, and there are some tiny particles at the outer surface of the tubes. As further increasing the temperature, more MBA monomer dissolved and participated in solution polymerization. As more particles formed in solution, the tube surface turned to be rougher, as shown in Figs. 2(c)–(e). If the amount of AIBN was further lowered to 0.0027 g (sample 6), the polymerization at 80°C gave only polymer particles without tubes (Fig. 2(f)). Considering the morphologies of the tubes, the optimal reaction temperature should be 65°C. In addition, Fig. 3 indicates that more products were obtained at higher reaction temperature.

The influence of RAFT reagent on the morphologies of the products is shown in Fig. 1(b) (sample 1) and Fig. S2 (sample 7–9). There are a lot of particles and few tubes in sample 7 without RAFT reagent. As increasing the amount of RAFT reagent, the tube surface became smoother and smoother. At the highest amount of RAFT reagent (sample 9), collapsed tubes with smooth surface were obtained. Considering the tube morphologies, the optimal amount of RAFT reagent should be 0.0130 g (sample 1). Because RAFT reagent was actually a chain transfer agent in the RAFT polymerization [37,38], at a lower amount of RAFT reagent, part of the free-radical chains could not be sealed by RAFT reagent and they initiated the conventional free-radical polymerization to form particles [31,32]. As increasing the amount of RAFT reagent, the formation of particles was gradually inhibited and the tube surface turned to be smoother. From Fig. S3, the weight of products decreased at higher amount of RAFT reagent.

At 65°C and 0.0130 g RAFT reagent, the RAFT polymerization of MBA crystals was carried out at different amount of AIBN (sample 1 and 10–14), all of which are higher than those used in xerogel fiber system [26]. As increasing the amount of AIBN, the tube wall became thicker and thicker with more and more particles being formed as shown in Fig. S4, while the weight of products increased gradually as indicated in Fig. S5. The formation of particles could also be attributed to the conventional free-radical polymerization at higher amount of AIBN.

It is interesting to discuss the size effect in the polymerization process. MBA crystals as the templates had much smaller total surface area compared with xerogel fibers. The solution RAFT polymerization of MBA gave soluble polymers initially. Because the templates had no sufficient surface to incorporate all the polymers, some of them stayed in solution and polymerized further into insoluble particles. As the particles attached onto the templates afterwards, polymer microtubes with rough surface were resulted. To obtained polymer microtubes with smooth surface, the RAFT polymerization of MBA crystals should be conducted at lower temperature to maintain a lower MBA concentration and restrain the solution polymerization. Meanwhile, a higher amount of AIBN should be adopted to achieve an adequate polymerization rate.

Table 2
Solubility of MBA in toluene at different temperature

T (°C)	Solubility (g/100 g solvent)	Dissolving percentage (%)
60	0.1613	10.8
70	0.1659	11.1
80	0.2116	14.1

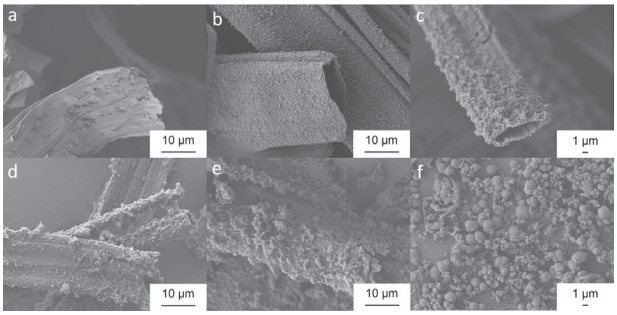

Fig. 2. SEM images of products prepared at different reaction temperature: (a) 60°C; (b) 65°C; (c) 70°C; (d) 75°C; (e) 80°C and (f) 80°C (sample 6).

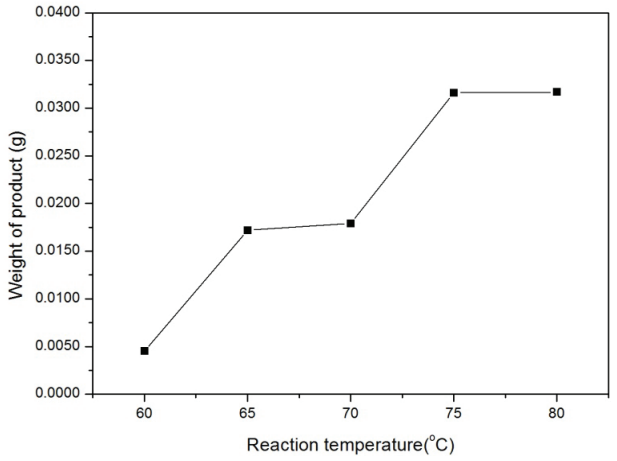

Fig. 3. Weight of products obtained at different reaction temperature.

3.2. Modification of polymer microtubes

Because the RAFT polymerization occurred at the outer surface rather than the interior part of MBA crystal. There should be considerable amount of unreacted acrylamide groups in the crosslinked tubes, especially at the inner surface. The tubes could be modified based on acrylamide groups. Considering the morphology of the tubes, sample 1 (defined as PMBA1 in the following) was selected for modification.

The swelling of PMBA1 in ethanol could be viewed by an optical microscope. As shown in Fig. 4, the diameter of a dried tube is 3.8 μm, and increases to 10.4 μm quickly after being immersed in ethanol. After partial evaporation of ethanol several minutes later, the tube shrinks to a diameter of 6.4 μm, as shown in Fig. 4(c). The swelling performance indicated that ethanol was an adequate solvent for the modification reaction because it increased the accessibility of acrylamide groups. So PMBA1 was dispersed in ethanol containing excessive TEPA for modification. After reacted at room temperature for 24 h, white modified product (defined as PMBA1-TEPA, Fig. S6) was obtained.

Fig. 5(a) shows the FTIR spectrum of PMBA1, where the broad peak at 3,299 cm^{-1} represents N–H stretching, and the peaks at 1,655, 1,528 and 1,216 cm^{-1} correspond to amide I, II and III bands, respectively. The peak at 808 cm^{-1} indicates the existence of residual double bonds, which should be attributed to the incomplete polymerization caused by the steric hindrance. Fig. 5(b) is the FTIR spectrum of PMBA1-TEPA. The main peaks are almost the same as those of PMBA1, indicating the backbone structures did not change during the modification process. A new peak at 1,031 cm^{-1} indicates the existence C–N of aliphatic amine. Moreover, the peak at 808 cm^{-1} is not noticed, indicating almost all acrylamide groups had reacted with TEPA. The characteristic peak of C=S of RAFT end groups at 1,074 cm^{-1} is also not noticed [39], which should be attributed to the cleavage of RAFT end groups by TEPA during the process [40]. These results confirmed that TEPA segments had incorporated into the tubes via aza-Michael addition between amine group as the Michael donor and acrylamide group as the Michael acceptor [34].

The elemental contents (Table S1) of both PMBA1 and PMBA1-TEPA were obtained by element analysis. After modification, the nitrogen content increased from 13.6% to 15.2% due to the incorporation of TEPA segments. Based on the change of nitrogen content, the weight content of TEPA in PMBA1-TEPA was estimated to be 7.3 wt%, corresponding to 0.39 mmol/g. While the sulfur content decreased from 8.5% to 5.5% due to the aminolysis of RAFT end groups [40]. The TGA curves (Fig. S7) of PMBA1 and PMBA1-TEPA indicate that the decomposition temperature decreased from 266°C to 227°C after modification, which should be attributed to the thermal breakage of weak C–N bond (the average bond energy of C–N is only 305.4 kJ/mol [41]) formed between acrylamide group and amino group.

Owing to the highly crosslinking structure, PMBA1 kept floating state in water. However, PMBA1-TEPA was hydrophilic due to the existence of many amino groups introduced by TEPA segments. After being treated in acid, the sample became more hydrophilic because of the formation of ammonium salt. PMBA1 kept shrinking state in water, while PMBA1-TEPA swelled considerably into transparent state in acidic water (Fig. S8).

To compare the hydrophilicity of PMBA1 and PMBA1-TEPA, the two samples were casted homogenously on glass plates and the water contact angles were measured on them. From Fig. 6, the water contact angles are 150.2° and 42.9° for the coatings of PMBA1 and PMBA1-TEPA, respectively. The rather low water contact angle of PMBA1-TEPA reveals its high hydrophilicity, which should be ascribed to the existence of TEPA segments in the sample.

The swelling ratios of PMBA1 and PMBA1-TEPA in some solvents were also measured to compare their swelling capacity. From the results in Fig. 7, both PMBA1 and PMBA1-TEPA

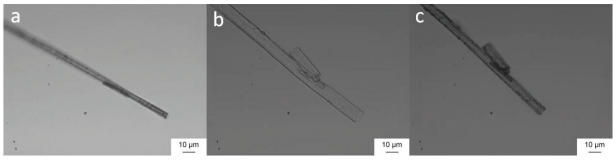

Fig. 4. Optical microscope images of a single tube of PMBA1: (a) under dried state; (b) swelling in ethanol and (c) after partial evaporation of ethanol.

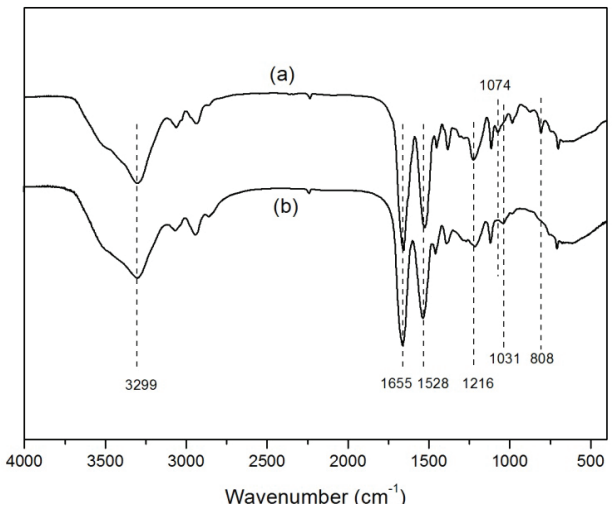

Fig. 5. FTIR spectra of: (a) PMBA1 and (b) PMBA1-TEPA.

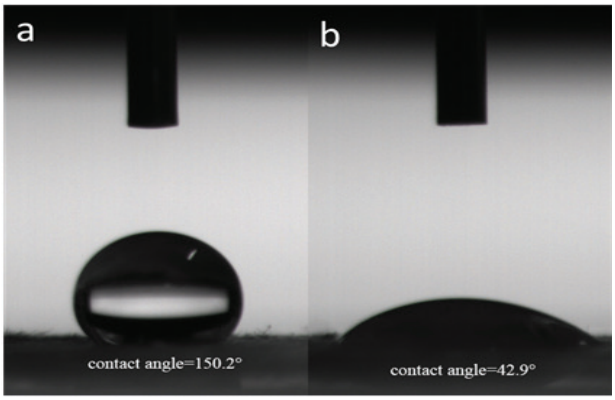

Fig. 6. Water contact angles of the coatings: (a) PMBA1 and (b) PMBA1-TEPA.

possess high swelling ratios in toluene and ethanol. But PMBA1-TEPA has much higher swelling ratios in neutral, acidic and alkaline water than PMBA1. These results further confirmed that PMBA1-TEPA acquired hydrophilicity after modification. In acidic water, the amino groups ionized into ammonium salt groups, thus improving the hydrophilicity further.

3.3. Adsorption and desorption

According to the literature results, TEPA functionalized nanosized magnetic polymer adsorbents could remove Cr(VI) from acidic water [9,10]. To investigate the adsorption capacity of Cr(VI), 0.0050 g PMBA1-TEPA was added into the aqueous solution of $K_2Cr_2O_7$ at pH values ranged from 2.0 to 11.5. The solution pH was adjusted by diluted hydrochloric acid or sodium hydroxide solution. The $K_2Cr_2O_7$ solution with initial concentration of 50 mg/L was applied in the measurement. After storage at 35°C for 24 h, the solution colour changed from yellow to colourless (Fig. S9) which indicated the concentration of Cr(VI) decreased significantly. Fig. 8 shows the adsorption capacity of PMBA microtubes and TEPA functionalized microtubes. The adsorption capacity of PMBA1-TEPA reached above 40 mg/g at pH 2, while PMBA was below 5 mg/g at all solution pH. It indicated that modification with TEPA enhanced the adsorption capacity of the tubes. From the curves in Fig. 8, the adsorption capacity of TEPA functionalized microtubes declined rapidly as the pH increased and maximal adsorption capacity was obtained at pH 2.5. On the other hand, the swelling ratios of functionalized microtubes did not have much difference between acid and alkaline environment as shown in Fig. 7. Therefore, the large difference of adsorption capacity was probably due to the pH, rather than the swelling. According to the literature [10], Cr(VI) existed in different forms depending to the pH values. At pH 2.5, Cr(VI) most existed as $HCrO_4^-$ and the amino groups were protonated, therefore, PMBA1-TEPA was able to absorb $HCrO_4^-$ ions via electrostatic attraction [10]. As pH value increased, Cr(VI) transferred into the form of CrO_4^{2-} and coordinate adsorption enhanced. Fig. 8 also implies that coordinate adsorption was weaker than electrostatic adsorption in this case, as adsorption capacity was much less in alkaline environment than in acid environment. As Fig. 9(a) shows, adsorption isotherm was plotted by equilibrium adsorption capacity

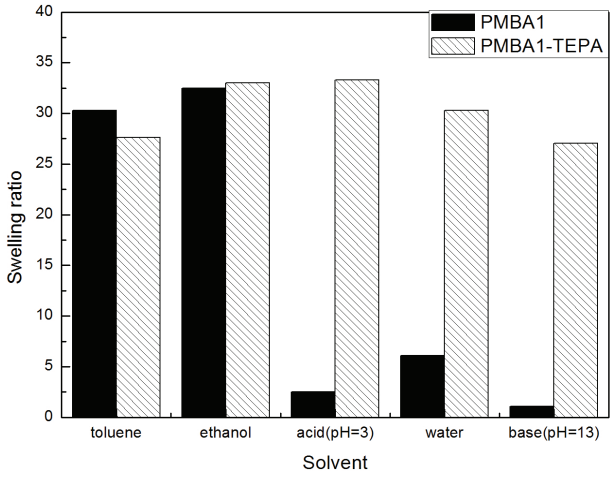

Fig. 7. Swelling ratios of the samples in different solvents.

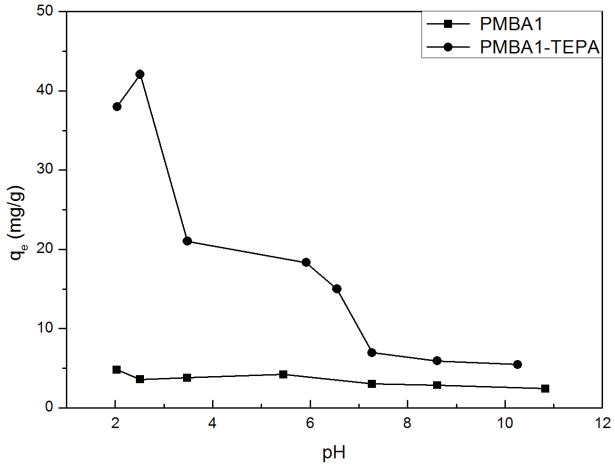

Fig. 8. Adsorption curves with different pH values.

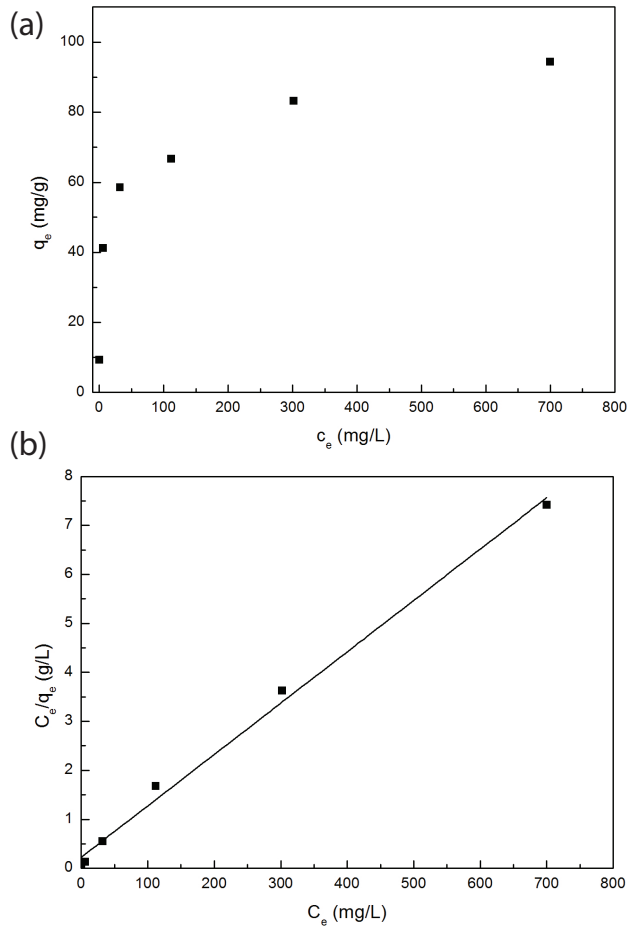

Fig. 9. Adsorption isotherm of Cr(VI) (a); Langmuir model fitting to the data (b).

Table 3
Model fitting for Langmuir and Freundlich

Model	Equation form	Parameter fitting	R^2 value
Langmuir	$\frac{c_e}{q_e}=\frac{1}{K_L q_m}+\frac{c_e}{q_m}$	q_m = 116.69, K_L = 0.09283	0.9965
Freundlich	$\log q_e = \log K_F + (1/n)\log c_e$	n = 3.3702, K_F = 26.546	0.9098

in different initial concentrations. The adsorption models of Langmuir and Freundlich were applied to the data as shown in Table 3. Langmuir model was more fit in this case, as the R^2 was 0.9934. As the initial concentration reached above 800 mg/L, the adsorption isotherm curve became flat, which indicated it nearly reached the maximum adsorption capacity as 95.2 mg/g in Langmuir model. Compared with most of the literature absorbents (Table S2) [42–49], PMBA-TEPA microtubes had relatively better adsorption capacity, which should be attributed to the high TEPA content. The total amount of primary and secondary amine groups in PMBA1-TEPA was calculated to be 1.95 mmol/g based on elemental analytic result. At pH 2.5, the amino groups were protonated and form complex with $HCrO^{4-}$ ions at stoichiometric ratio of 1:1 [10]. If all amine groups were available for combining with Cr(VI), the maximum adsorption capacity could reach 101.4 mg/g, corresponding well to 95.2 mg/g in Langmuir model. This performance should make PMBA1-TEPA suitable as an excellent absorbent for Cr(VI).

Because of the large size, PMBA-TEPA microtubes could be separated from Cr(VI) solution simply via filtration. Since the microtubes had low adsorption capacity in alkaline environment, we can choose sodium hydroxide solution for desorption. On the other hand, Cr(VI) might coordinate with other strong ligands and desorbed from microtubes. As Fig. 10 showed, different solutions were used as desorption agents. Among them, 0.1 mol/L NaOH solution had the highest desorption capacity. $NH_3{\cdot}H_2O$ exhibited some effect as well. Water and pyridine were not good desorption agents in this test. So that, 0.1 mol/L NaOH solution was used to desorb Cr(VI) in the following experiments. The adsorption and desorption processes could also be observed by naked eyes. After adsorbing at pH 2.5 for 24 h, the colour of solution became lighter and the microtubes turned dark yellow from white. After desorption at pH 13 for 24 h, the microtubes became white again.

Recycling performance was an important property for adsorbents. To determine the recycling performance of PMBA-TEPA microtubes, 50 mg/L Cr(VI) solution and 0.1 mol/L NaOH solution were used for adsorption and desorption, respectively. As shown in Fig. 11, after cycling for four times, adsorption capacity decreased slowly from 37 to 21 mg/g, while adsorption efficiency decreased from 60% to 35%, indicating PMBA1-TEPA microtubes could not completely desorb in NaOH solution. Some of TEPA group combined with Cr(VI) by coordinate effect, so that this part of TEPA group could not contribute in the next adsorption process. As a result, adsorption capacity decreased to some extent as shown in Fig. 11.

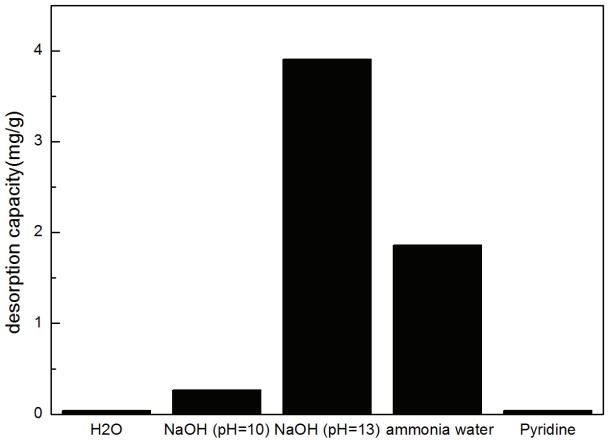

Fig. 10. Desorption capacity with different desorption agents.

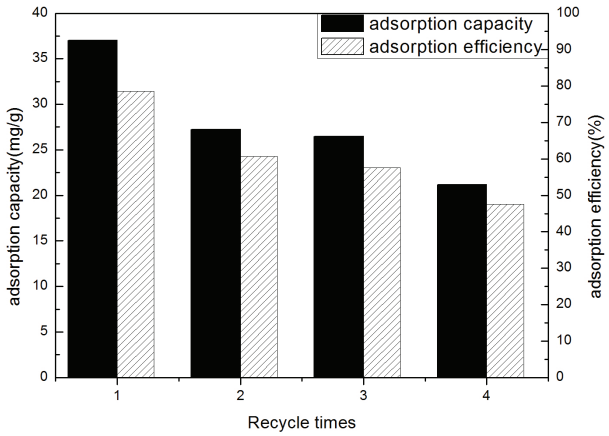

Fig. 11. Recycling performance of modified microtubes.

4. Conclusions

In summary, we have found that functional macroscopic polymer microtubes could be fabricated successfully via two preparation steps, including RAFT polymerization of MBA crystals and modification of the resulting tubes. Because of the large size of the crystals, low temperature and high amount of initiator should be adopted to achieve suitable morphologies for the tubes. Owing to the residual acrylamide groups, the polymer microtubes were able to react with TEPA in ethanol. The existence of TEPA segments in the modified sample was confirmed by various techniques. With considerable amino groups on the tubes, the modified sample displayed high hydrophilicity and excellent adsorption

capacity for Cr(VI). The acid environment was benefit for adsorption and maximal adsorption capacity was obtained at pH 2.5. The maximum adsorption capacity reached 95.2 mg/g, according to Langmuir model. Cr(VI)-adsorbed tubes could desorb in alkaline environment. The modified microtubes displayed good recycling performance, although the adsorption capacity slightly decreased during cycling. This investigation described a simple preparation process for functional macroscopic PMBA microtubes. The excellent adsorption capacity and good recycling performance should make the tubes suitable as absorbent for Cr(VI).

Acknowledgements

This work was supported by the National Natural Science Foundation of China (No. 21574074) and National Basic Research Program of China (973 plan, No. 2014CB932202).

References

[1] A. Zhitkovich, Chromium in drinking water: sources, metabolism, and cancer risks, Chem. Res. Toxicol., 24 (2011) 1617−1629.
[2] H.N.E. Mahmud, A.K.O. Huq, R.B. Yahya, ChemInform abstract: the removal of heavy metal ions from wastewater/aqueous solution using polypyrrole based adsorbents: a review, RSC Adv., 6 (2016) 14778–14791.
[3] P.L. Ai, A.Z. Aris, A review on economically adsorbents on heavy metals removal in water and wastewater, Rev. Environ. Sci. Biotechnol., 13 (2014) 163–181.
[4] P.S. Kulkarni, V. Kalyani, V.V. Mahajani, Removal of hexavalent chromium by membrane-based hybrid processes, Ind. Eng. Chem. Res., 46 (2007) 8176–8182.
[5] D.D. Maksin, A.B. Nastasović, A.D. Milutinović-Nikolić, L.T. Suručić, Z.P. Sandić, R.V. Hercigonja, A.E. Onjia, Equilibrium and kinetics study on hexavalent chromium adsorption onto diethylene triamine grafted glycidyl methacrylate based copolymers, J. Hazard. Mater., 209–210 (2012) 99–110.
[6] V. Eyupoglu, Alkyl chain structure-dependent separation of Cr(VI) from acidic solutions containing various metal ions using liquid–liquid solvent extraction by butyl-based imidazolium bromide salts, Desal. Wat. Treat., 57 (2016) 17774–17789.
[7] S. Koushkbaghi, P. Jafari, J. Rabiei, Fabrication of PET/PAN/GO/Fe_3O_4 nanofibrous membrane for the removal of Pb(II) and Cr(VI) ions, Chem. Eng. J., 301 (2016) 42–50.
[8] L. Lei, W. Cai, J. Zhou, Facile synthesis of boehmite/PVA composite membrane with enhanced adsorption performance towards Cr(VI), J. Hazard. Mater., 318 (2016) 452–459.
[9] W. Cai, L. Tan, J. Yu, Synthesis of amino-functionalized mesoporous alumina with enhanced affinity towards Cr(VI) and CO_2, Chem. Eng. J., 239 (2014) 207–215.
[10] H. Shen, J. Chen, H. Dai, New insights into the sorption and detoxification of chromium(VI) by tetraethylenepentamine functionalized nanosized magnetic polymer adsorbents: mechanism and pH effect, Ind. Eng. Chem. Res., 52 (2013) 12723–12732.
[11] G. Moad, E. Rizzardo, S.H. Thang, RAFT polymerization and some of its applications, Chem. Asian J., 8 (2013) 1634–1644.
[12] A. Gregory, M.H. Stenzel, Complex polymer architectures via RAFT polymerization: from fundamental process to extending the scope using click chemistry and nature's building blocks, Prog. Polym. Sci., 37 (2012) 38–105.
[13] C. Boyer, M.H. Stenzel, T.P. Davis, Building nanostructures using RAFT polymerization, J. Polym. Sci., Part A: Polym. Chem., 49 (2011) 551–595.
[14] W.M. Wan, C.Y. Pan, One-pot synthesis of polymeric nanomaterials via RAFT dispersion polymerization induced self-assembly and re-organization, Polym. Chem., 1 (2010) 1475–1484.
[15] C. Boyer, V. Bulmus, T.P. Davis, V. Ladmiral, J. Liu, S. Perrier, Bioapplications of RAFT polymerization, Chem. Rev., 109 (2009) 5402–5436.
[16] O.J. Dautel, M. Robitzer, J.P. Lere-Porte, F. Serein-Spirau, J.J.E. Moreau, Self-organized ureido substituted diacetylenic organogel. Photopolymerization of one-dimensional supramolecular assemblies to give conjugated nanofibers, J. Am. Chem. Soc., 128 (2006) 16213–16223.
[17] V. Magdanz, M. Guix, F. Hebenstreit, O.G. Schmidt, Dynamic polymeric microtubes for the remote-controlled capture, guidance, and release of sperm cells, Adv. Mater., 28 (2016) 4084–4089.
[18] E.N. Savariar, K. Krishnamoorthy, S. Thayumanavan, Molecular discrimination inside polymer nanotubules, Nat. Nanotechnol., 3 (2008) 112–117.
[19] H. Fana, X.L. Yua, Y.H. Long, X.Y. Zhang, H.F. Xiang, C.T. Duan, N. Zhao, X.L. Zhang, J. Xu, Preparation of kapok–polyacrylonitrile core–shell composite microtube and its application as gold nanoparticles carrier, Appl. Surf. Sci., 258 (2012) 2876–2882.
[20] S.I. Cho, S.B. Lee, ChemInform abstract: fast electrochemistry of conductive polymer nanotubes: synthesis, mechanism, and application, Acc. Chem. Res., 39 (2008) 699–707.
[21] F. Massuyeau, J.L. Duvail, H. Athalin, J.M. Lorcy, S. Lefrant, J. Wéry, E. Faulques, Elaboration of conjugated polymer nanowires and nanotubes for tunable photoluminescence properties, Nanotechnology, 20 (2009) 155701.
[22] J. Jang, H. Yoon, Facile fabrication of polypyrrole nanotubes using reverse microemulsion polymerization, Chem. Commun., 9 (2003) 720–721.
[23] I.G. Loscertales, A. Barrero, M. Márquez, R. Spretz, R. Velarde-Ortiz, G. Larsen, Electrically forced coaxial nanojets for one-step hollow nanofiber design, J. Am. Chem. Soc., 126 (2004) 5376–5377.
[24] Q. Li, L.M. Tang, Y. Jiao, Influence of comonomers on the transformation of MBA gel fibers into polymer micro-tubes via RAFT polymerization, Acta Polym. Sin., 21 (2014) 1135–1142.
[25] Q. Li, L.M. Tang, Y. Liang, Preparation of polymer microtubes *via* RAFT polymerization of *N*,*N*′-methylene bisacrylamide gel fibers, Chem. J. Chin. Univ., 34 (2013) 1542–1546.
[26] Y.Q. Zhang, L.M. Tang, Q. Li, Preparation of polymer microtubes via RAFT polymerization of sole MBA xerogel fibers, Acta Chem. Sin., 73 (2015) 126–130.
[27] Q. Li, L.M. Tang, Y. Xia, B.T. Li, Direct transformation of *N*,*N*′-methylene bisacrylamide self-assembled fibers into polymer microtubes via RAFT polymerization, Macromol. Rapid Commun., 34 (2013) 185–189.
[28] Q. Li, L.M. Tang, One-step synthesis of polymer micro-tubes tethered by polymer nanowire networks via RAFT polymerization of *N*,*N*′-methylene bisacrylamide xerogel fibers in toluene and ethanol mixed solution, J. Polym. Sci., Part A: Polym. Chem., 52 (2014) 1862–1868.
[29] Q. Li, Y. Wang, L. M. Tang, Fabrication of fluoropolymer microtubes via RAFT copolymerization of *N*,*N*′-methylene bisacrylamide gel fibers and fluoromonomer, Chem. Asian J., 10 (2015) 1363–1369.
[30] L. Liu, C.L. Wu, J.C. Zhang, M.M. Zhang, Y.W. Liu, X.J. Wang, G.Q. Fu, Controlled polymerization of 2-(diethylamino) ethyl methacrylate and its block copolymer with *N*-isopropylacrylamide by RAFT polymerization, J. Polym. Sci., Part A: Polym. Chem., 46 (2010) 3294–3305.
[31] N. Ide, T. Fukuda, Nitroxide-controlled free-radical copolymerization of vinyl and divinyl monomers. 2. Gelation, Macromolecules, 32 (1999) 95–99.
[32] Q.F. Liu, P. Zhang, A.X. Qing, Y.X. Lan, M.G. Lu, Poly(*N*-isopropylacrylamide) hydrogels with improved shrinking kinetics by RAFT polymerization, Polymer, 47 (2006) 2330–2336.
[33] Y. Xia, Y. Wang, K. Chen, L.M. Tang, A facile approach to fabricate functional 3D macroscopic silica microtube networks using *N*,*N*′-methylenediacrylamide organogel as template, Chem. Commun., 41 (2008) 5113–5115.
[34] K. Surendra, N.S. Krishnaveni, R. Sridhar, K.R. Rao, β-Cyclodextrin promoted aza-Michael addition of amines

to conjugated alkenes in water, Tetrahedron Lett., 47 (2006) 2125–2127.
[35] N. Aoyagi, T. Endo, Functional RAFT agents for radical-controlled polymerization: quantitative synthesis of trithiocarbonates containing functional groups as RAFT agents using equivalent amount of CS_2, J. Polym. Sci., Part A: Polym. Chem., 47 (2009) 3702–3709.
[36] A.D. Eaton, L.S. Clesceri, A.E. Greenberg, Standard Methods for the Examination of Water and Wastewater: Supplement to the Sixteenth Edition, American Public Health Association (APHA), American Water Works Association (AWWA), Water Pollution Control Federation (WPCF), Washington, D.C., USA, 2000.
[37] J. Chiefari, Y.K.B. Chong, F. Ercole, J. Krstina, J. Jeffery, T.P.T. Le, R.T.A. Mayadunne, G.F. Meijs, C.L. Moad, G. Moad, E. Rizzardo, S.H. Thang, Living free-radical polymerization by reversible addition–fragmentation chain transfer: the RAFT process, Macromolecules, 31 (1998) 5559–5562.
[38] G. Moad, J. Chiefari, B.Y. Chong, J. Krstina, R.T. Mayadunne, A. Postma, E. Rizzardo, S.H. Thang, Living free radical polymerization with reversible addition–fragmentation chain transfer (the life of RAFT), Polym. Int., 49 (2000) 993–1001.
[39] J.T. Lai, D. Filla, R. Shea, Functional polymers from novel carboxyl-terminated trithiocarbonates as highly efficient RAFT agents, Macromolecules, 35 (2002) 6754–6756.
[40] J.T. Xu, J.P. He, D.Q. Fan, X.J. Wang, Y.L. Yang, Aminolysis of polymers with thiocarbonylthio termini prepared by RAFT polymerization: the difference between polystyrene and polymethacrylates, Macromolecules, 39 (2006) 8616–8624.
[41] Q.Y. Xing, W.W. Pei, R.Q. Xu, J. Xu, Basic Organic Chemistry, Higher Education Press, Beijing, 2010, p. 19.
[42] R. Nithya, T. Gomathi, P.N. Sudha, Removal of Cr(VI) from aqueous solution using chitosan-*g*-poly(butyl acrylate)/silica gel nanocomposite, Int. J. Biol. Macromol., 87 (2016) 545–554.
[43] A.G. Khiratkar, S.S. Kumar, P.R. Bhagat, Designing a sulphonic acid functionalized benzimidazolium based poly(ionic liquid) for efficient adsorption of hexavalent chromium, RSC Adv., 6 (2016) 37757–37764.
[44] M.L. Chen, Y.N. Zhao, D.W. Zhang, Y. Tian, J.H. Wang, The immobilization of hydrophilic ionic liquid for Cr(VI) retention and chromium speciation, J. Anal. At. Spectrom., 25 (2010) 1688–1694.
[45] S.P. Bayen, P. Chowdhury, Synthesis of novel aniline immobilized silica gel for the selective extraction of Cr(III), Desal. Wat. Treat., 52 (2014) 1550–1559.
[46] B. Qui, J. Guo, X. Zhang, D. Sun, H. Gu, Q. Wang, H. Wang, X. Wang, X. Zhang, B.L. Weeks, Z. Guo, S. Wei, Polyethylenimine facilitated ethyl cellulose for hexavalent chromium removal with a wide pH range, ACS Appl. Mater. Interfaces, 6 (2014) 19816–19824.
[47] S.M. Xu, S. Zhang, R. Lu, J.Z. Yang, C.X. Cui, Study on adsorption behavior between Cr(VI) and crosslinked amphoteric starch, J. Appl. Polym. Sci., 89 (2003) 263–267.
[48] M.T. Rahman, Z. Barikbin, A.Z.M. Badruddoza, P.S. Doyle, S.A. Khan, Monodisperse polymeric ionic liquid microgel beads with multiple chemically switchable functionalities, Langmuir, 29 (2013) 9535–9543.
[49] D. Duranoglu, A.W. Trochimczuk, U. Beker, Kinetics and thermodynamics of hexavalent chromium adsorption onto activated carbon derived from acrylonitrile-divinylbenzene copolymer, Chem. Eng. J., 187 (2012) 193–202.

Supporting information

Fig. S1. Photograph of macroscopic PMBA microtubes.

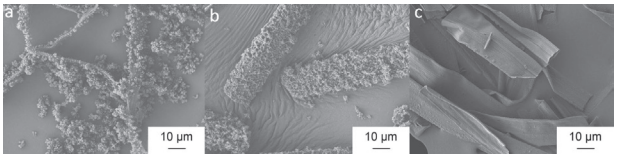

Fig. S2. SEM images of products obtained at different amount of RAFT reagent: (a) 0 g; (b) 0.0065 g and (c) 0.0200 g.

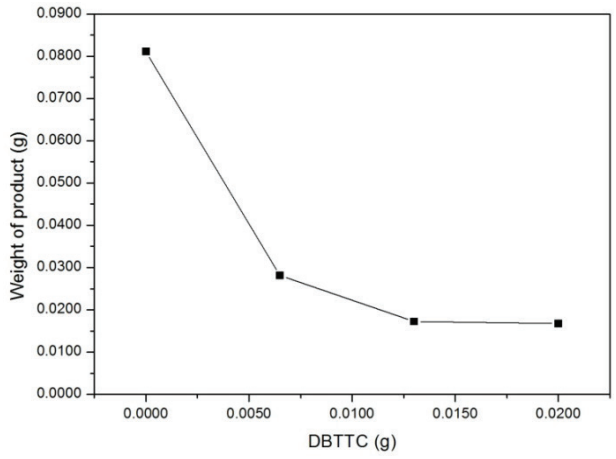

Fig. S3. Weight of products obtained at different amount of RAFT reagent.

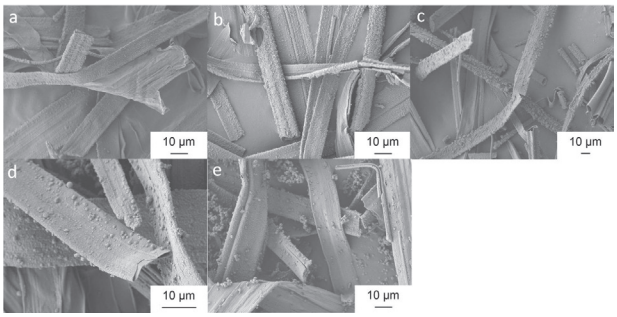

Fig. S4. SEM images of products obtained at different amount of AIBN: (a) 0.0040 g; (b) 0.0060 g; (c) 0.0120 g; (d) 0.0150 g and (e) 0.0180 g.

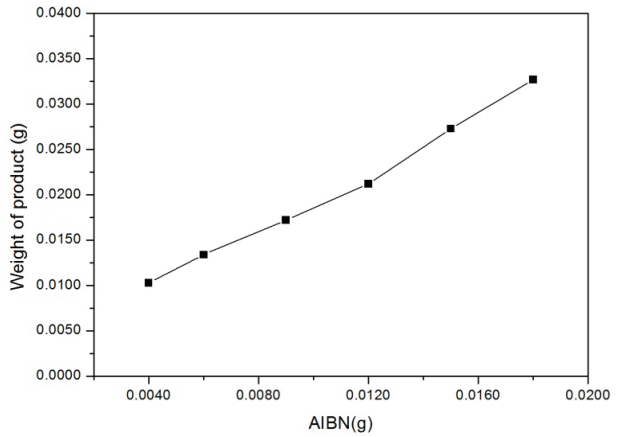

Fig. S5. Weight of products obtained at different amount of AIBN.

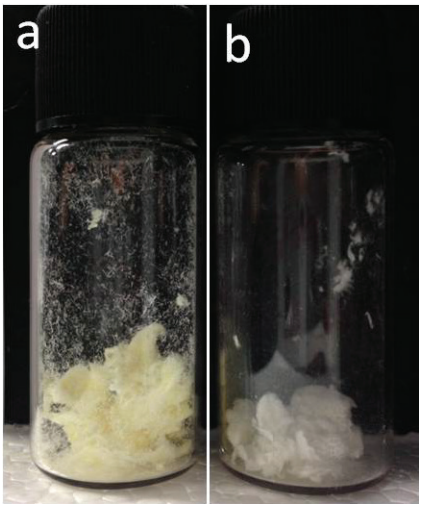

Fig. S6. Appearance of PMBA1 (a) and PMBA1-TEPA (b).

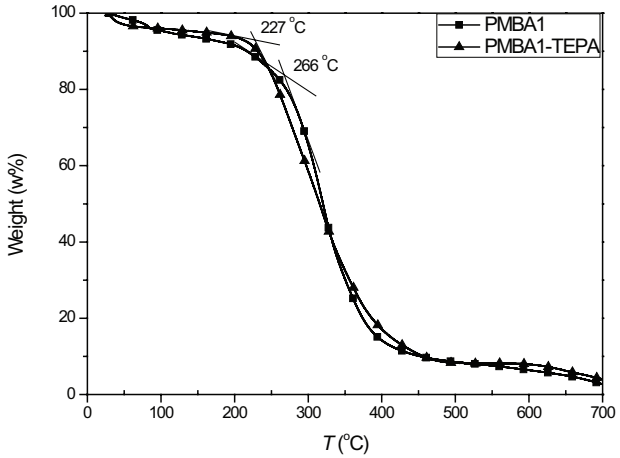

Fig. S7. Curves of weight loss measured by TGA.

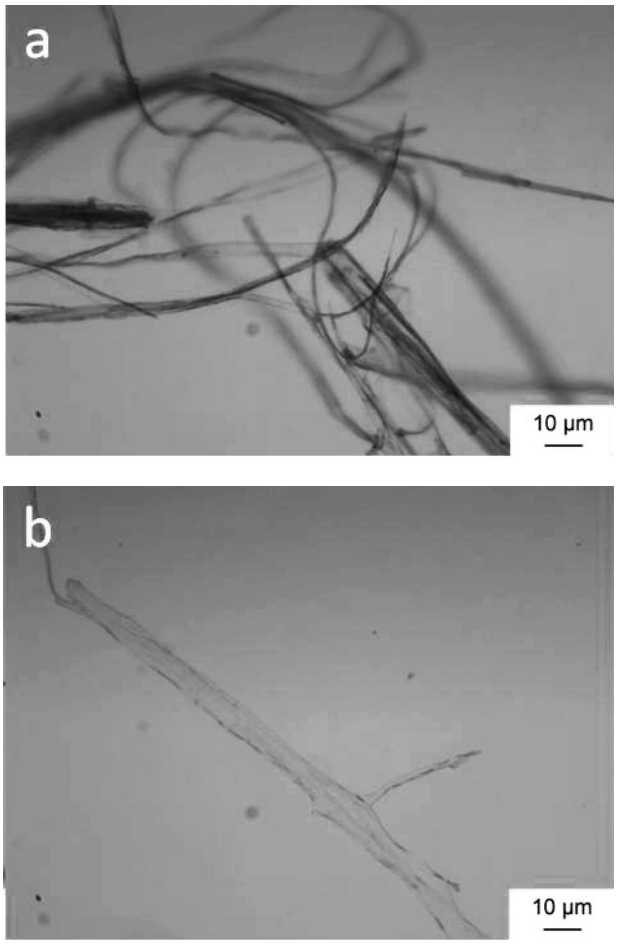

Fig. S8. Optical microscope images of different samples in water: (a) PMBA1 and (b) PMBA1-TEPA after acid treatment.

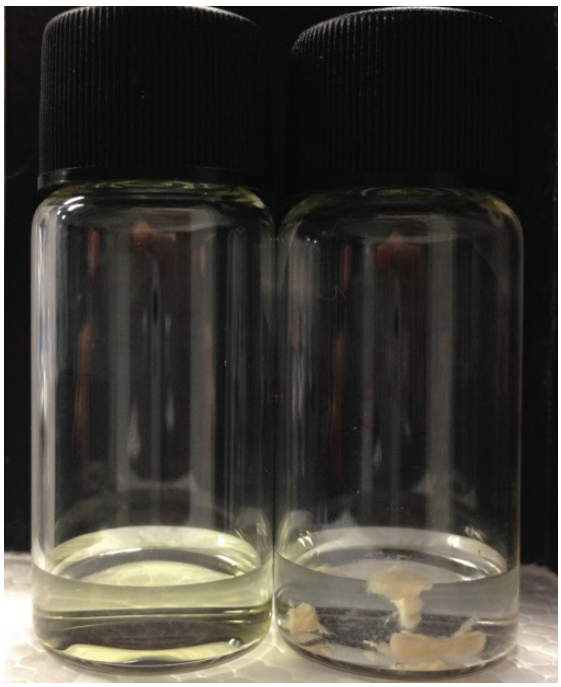

Fig. S9. Photographs of Cr(VI) solutions: original (left) and after being treated by PMBA1-TEPA (right).

Table S1
Elemental contents of PMBA1 and PMBA1-TEPA

Sample	N (wt%)	C (wt%)	S (wt%)
PMBA1	13.6	54.2	8.5
PMBA1-TEPA	15.2	53.6	5.5

Table S2
Comparison the maximal adsorption capacity for Cr(VI)

Adsorbents	Maximal adsorption capacity (mg/g)	References
Chitosan-*g*-poly(butyl acrylate)/silica gel nanocomposite	55.7	42
Poly(ionic liquid) (SBPIL)	40.8	43
Hydrophilic ionic liquid (PVC-NmimCl)	23.2	44
Aniline immobilized silica gel	4.7	45
Polyethylenimine facilitated ethyl cellulose	36.8	46
Crosslinked amphoteric starches	28.8	47
Polymeric ionic liquid microgel beads	74	48
Activated carbon	81.5	49
PMBA–TEPA microtubes	95.2	This article